INFALLING ENVELOPES AND PRE-MAIN SEQUENCE DISKS

NASA Grant NAGW-2306

Annual Report No. 4

For the period 1 September 1995 through 31 August 1996

Principal Investigator

Lee W. Hartmann

October 1996

Prepared for
National Aeronautics and Space Administration
Washington, D.C. 20546

Smithsonian Institution
Astrophysical Observatory
Cambridge, Massachusetts 02138

The Smithsonian Astrophysical Observatory
is a member of the
Harvard-Smithsonian Center for Astrophysics

The NASA Technical Officer for this Grant is Dr. Patricia Rogers, Code SLC, Headquarters, National Aeronautics and Space Administration, Washington, D.C. 20546

INFALLING ENVELOPES AND PRE-MAIN SEQUENCE DISKS

Annual Report 9/1/95 - 8/31/96, NAGW-2306, Hartmann et al.

The goal of this project is to understand the observed infrared emission of young stellar objects, and explore the implications of this emission for the evolution of dusty envelopes and circumstellar disks. We are using sophisticated radiative transfer methods to compare models with observations, thereby making critical tests of the standard picture of low-mass star formation.

SHEET MODELS OF PROTOSTELLAR COLLAPSE

Observations (Myers et al. 1991) indicate that protostellar molecular cloud cores are not spherically symmetric, but are noticably elongated. To investigate the potential effects of initial protostellar cloud geometry on collpase, in a previous paper supported by this grant (Hartmann *et al.* 1994) we presented an initial exploration of protostellar collapse from a flattened cloud. We considered the time-dependent axisymmetric evolution of a marginally Jeans-unstable region in an isothermal, non-magnetic, non-rotating, self-gravitating sheet. An important aspect of collapse from a sheet, which differs qualitatively from contraction of an initially spherical distribution of material, is the appearance of two "bipolar" cavities on either side of the central plane of the sheet (bottom panels of Figure 1). The cavities result simply because the regions closest to the central mass fall in before material from distant regions in the plane of the sheet can reach the center. Similar infall cavities were found in the simulations of the collapse of a rotating, magnetized filamentary cloud by Nakamura *et al.* (1995).

We published calculations aimed at addressing some of the observational consequences of the sheet collapse model (Hartmann, Calvet, & Boss 1996). To calculate the predicted emission from sheet collapse models in a reasonably accurate way, we needed to extend the results of Paper I to finer spatial grids near the central protostar than generally feasible with hydrodynamic calculations for the entire envelope. We also had to modify the results of Paper I to include rotation, because the angular momentum of the collapsing cloud plays a crucial role in determining the extinction through the inner envelope (see discussion in Adams *et al.* 1987). Our strategy is to assume that rotation plays a small role at large scales, as also assumed in the TSC solutions, so that we can use the results of Paper I to calibrate our large-scale density structure, while modifying the solution on small scales to account for the angular momentum barrier. Here we develop an analytic model which accounts for rotation and can also be divided into a sufficiently fine spatial grid for the calculation of the inner envelope emission.

Figure 1 compares the simulation in Paper I at one point in time with the analytic sheet collapse models. The overall properties of the density distribution are approximately reproduced with the appropriate choice of the parameter η. The agreement is reasonable, especially when one considers that this solution is really only valid for regions much smaller than than the outer cloud radius. The model works better at later times than at earlier times, partly because there are substantial departures from radial free-fall motions during the initial stages of collapse.

Figure 2 shows J band (1.25μm) images and polarization patterns for sheet models with the above parameters and $\eta = 1, 2, 3, 4$, viewed at an inclination of $i = 60°$ to the line of sight.

The images have been convolved with a gaussian point spread function with a full-width at half-maximum of one pixel (= 28 AU) to smooth the results slightly.

These images show that the sheet collapse models naturally produce reflection nebulae which appear to have large opening angles. As discussed in §3.2, values of $\eta \sim 2.5 - 3.5$ are characteristic of the envelope density distribution during the main infall phase, which would produce very open cavities. Since η should increase with increasing time, the sequence shown in Figure 5 corresponds to a time sequence, suggesting that the opening angle of reflection nebulae should increase with increasing age.. The polarization patterns are generally centrosymmetric, with some departures near the highest extinction regions from multiple scattering (Whitney & Hartmann 1993).

Our results suggest that collapse cavities can naturally explain the morphological appearance of many reflection nebulae around young stars on small distance scales without requiring initially diverging outflows. Sheet collapse models can simultaneously explain small-scale reflection nebula morphologies and dust envelope emission properties of many young stellar objects more easily than the standard spherical collapse models. The sheet collapse picture suggests that protostars, i.e. young stellar objects still accreting a large fraction of their mass from infalling envelopes, may be optically visible over a substantial range of system inclinations to the line of sight. These results may be especially relevant to cases where fragmentation and collapse has been triggered by an external impulse, such as a shock wave.

As another example of how sheet infall models can eliminate the discrepancy between SED fitting and the reflection nebula morphology, we applied our models to the flat spectrum T Tauri star HL Tau. This optically-visible object has a very large infrared excess, so that the SED is relatively flat between about 3 and 100 μm. Calvet *et al.* (1994) showed that the mid- to far-infrared emission of HL Tau could be reproduced by infalling envelope models with typical parameters of Class I stars in Taurus; in particular, the SEDs of 04016+2610 and HL Tau are very similar. The infall rate needed to explain the far-infrared emission is also consistent with analyses of near-infrared scattered light by Beckwith *et al.* (1989), redshifted C_2 absorption (Grasdalen *et al.* 1989), and ^{13}CO radio interferometer maps (Hayashi *et al.* 1993). However, as in the case of 04016+2610, the Calvet *et al.* envelope model for the SED HL Tau was unsatisfactory in that it demanded a narrow polar envelope hole, with a half-angle $\sim 10°$. In contrast, the observed optical nebula has a quite large apparent opening half-angle, $\approx 45°$ (e.g., Gledhill & Scarrott 1989; Stapelfeldt *et al.* 1995), but a cavity model with a streamline hole, adopting an opening angle of this magnitude, would result in an unacceptable fit to the SED.

We showed that sheet collapse models can explain the SED, the scattered light image, and the near-infrared polarization and photocenter shift with wavelength in HL Tau. Our constraints are (1) an infall rate comparable to that derived by Hayashi *et al.* (1993) from independent analysis of the ^{13}CO interferometer maps, and (2) a centrifugal radius R_c smaller than the $\sim$ 140 AU outer disk radius suggested by the sub-mm interferometry of Lay *et al.* (1994). (We expect that the disk, if anything, will have spread to larger radii than R_c; Cassen & Moosman 1981). The first constraint is straightforwardly met, since we assume $\dot{M} = 4 \times 10^{-6} M_\odot yr^{-1}$, the typical mean value of infall rates found for Taurus Class I sources by Kenyon *et al.* (1993a), essentially equal to the infall rate derived by Hayashi *et al.* (1993), and sufficiently close to the $\dot{M} \sim 6 \times 10^{-6} M_\odot yr^{-1}$ we found for the "plateau" phase of infall in our isothermal numerical simulation. We also adopt $R_c = 50$ AU for concreteness, although the precise value adopted is not critical given the sensitivity of the results to inclination. Finally, since HL Tau is apparently surrounded by an envelope with a mass accretion rate comparable to that observed and predicted for the main infall phase, we might

expect "intermediate" values of $\eta \sim 2 - 3$.

Figure 3 compares SEDs calculated for sheet collapse models with $\eta = 2, 3$ to the observed SED of HL Tau. The $\eta = 2$ model fits the long-wavelength infrared emission better than the $\eta = 3$ model, which exhibits too much flux. Once again we emphasize that our assumption of a spherical temperature distribution may cause the comparison with the $\eta = 3$ model to appear worse than it actually should. In a more accurate radiative equilibrium calculation, the polar, low density, regions will be hotter because radiation will preferentially escape in these directions; the equatorial, densest regions, will become cooler. Since the far infrared emission comes from optically-thin regions, and most of the emitting envelope in a sheet model is in the equatorial region, a sheet model would probably have lower temperatures and therefore lower far-infrared fluxes. This conjecture is supported by the modelling of Chick *et al.* (1995), who considered infalling envelopes with cavities; using a Rosseland mean opacity, Chick *et al.* found that the equatorial envelope temperatures could be as much as a factor of two lower than the spherical case for large cavities, such as implicit in the $\eta = 3$ model.

We also showed that the depth of the 10μm silicate feature is very sensitive to the system inclination. In both models the best comparisons occur for $i \sim 65°$, or $\mu \sim 0.4$. Our models show that the silicate feature depth is so geometry-dependent that it is unlikely to be a reliable measure of envelope optical depth.

Figure 4 shows scattered light images for the $\eta = 2, 3$ models at appropriate inclinations. The observed HL Tau J-band polarization can be reproduced at $\eta = 2$ if $\mu = 0.5$ or at $\eta = 3$ if $\mu = 0.3$. The true system inclination is unknown, but the aspect ratio of the molecular gas observed by Sargent & Beckwith (1991) and Hayashi *et al.* (1993) suggests $\mu \approx 0.5$. The appearance of the large-scale scattered light nebula is perhaps better matched by $\eta = 3$ models, which provide reasonable agreement with the wide opening angle suggested by large-scale images, although the HST images show fine-scale structure in the nebula (Stapelfeldt *et al.* 1995) that cannot possibly be explained by the simple axisymmetric model used here.

The Calvet *et al.* spherical collapse model for HL Tau demanded a narrow outflow hole, because an evacuated hole with a wide opening angle eliminates the mid-infrared excess as discussed above (see also Figure 6 of Calvet *et al.* 1994). With such a narrow cavity, the reflection nebula morphology would look quite different than observed. The η models do not have the same problem because the envelope cavity is not completely evacuated of dust; even small amounts of material can provide the required mid-infrared emission.

Beckwith & Birk (1995) showed that the position of the peak near-infrared intensity in HL Tau shifts in position by about $0.53 \pm 0.07\, arcsec \sim 74$ AU between 2.12 μm and 1.25 μm; this result was confirmed and extended in wavelength by Weintraub, Kastner, and Whitney (1995). Both sets of authors interpret this shift as due to a combination of an extended scattered light nebula seen behind a medium with an extinction gradient. Beckwith & Birk suggested that the extincting medium might be either an infalling envelope or the extended atmosphere of a circumstellar disk; Weintraub *et al.* favored the former explanation.

Our models also predict photocenter shifts, since the central star is hidden by a scattering, absorbing envelope with a substantial spatial gradient in its column density. We convolved the models with a $1\, arcsec$ gaussian point spread function to be more directly comparable to the ground-based measurements. For $\eta = 2$, we find shifts at J of 16 AU and 53 AU at $\mu = 0.5$ and $\mu = 0.4$, respectively; for $\eta = 3$, the shifts at J are 10 AU and 63 AU at $\mu = 0.4$ and $\mu = 0.3$, respectively. The two largest of these shifts are reasonably consistent with the observations,

although the polarizations predicted by the large photocenter shift models, 11% and 19%, are somewhat larger than observed.

Thus, in general our models were quite successful in explaining many observed features of protostellar sources. Since protostellar clouds are not spherically-symmetric, our results should be generally applicable to such sources.

THE STRUCTURE AND EMISSION OF ACCRETION DISKS IRRADIATED BY INFALLING ENVELOPES

In a recently accepted paper (D'Alessio et al. 1997) we calculated the emission from steady viscous disks heated by radiation from an opaque infalling protostellar envelope. For typical envelope parameters used to explain the spectral energy distributions of protostellar sources, we found that the envelope heating raises the outer disk temperature dramatically. The resulting temperature distribution in the disk is a complicated function of both radial distance and vertical height above the disk midplane. We showed that the visibility flux at $\lambda = 0.87\ mm$ and the spectral energy distribution from submm to radio wavelengths of the flat-spectrum T Tauri star HL Tau can be explained by emission from an accretion disk irradiated by its infalling envelope, whereas thermal emission from an infalling envelope or radiation from a steady viscous accretion disk cannot explain the observations. Our results suggest that the radiation fields of collapsing protostellar envelopes may strongly affect the structure of pre-main sequence accretion disks.

DISK ACCRETION AND THE STELLAR BIRTHLINE

In a recently accepted paper (Hartmann, Cassen, & Kenyon 1997), we presented a simplified analysis of some effects of disk accretion on the early evolution of fully-convective, low-mass pre-main sequence stars. Our analysis builds on the previous seminal work of Stahler (1988) but differs in that the accretion of material occurs over a small area of the stellar surface, such as through a disk or magnetospheric accretion column, so that most of the stellar photosphere is free to radiate to space. This boundary condition is similar to the limiting case considered by Palla & Stahler (1992) for intermediate-mass stars.

We argued that for a wide variety of disk mass accretion rates, material will be added to the star with relatively small amounts of thermal energy. Protostellar evolution calculated assuming this "low-temperature" limit of accretion generally follows the results of Stahler because of the thermostatic nature of deuterium fusion, which prevents protostars from contracting below a "birthline" in the HR diagram. Our calculated protostellar radii tend to fall below Stahler's at higher masses; the additional energy loss from the stellar photosphere in the case of disk accretion tends to make the protostar contract. The low-temperature disk accretion evolutionary tracks never fall below the deuterium-fusion birthline until the internal deuterium is depleted, but protostellar tracks can lie above the birthline in the HR diagram if the initial radius of the protostellar core is large enough, or if rapid disk accretion (such as might occur during FU Ori outbursts) adds significant amounts of thermal energy to the star. These possibilities cannot be ruled out by either theoretical arguments or observational constraints at present, so that individual protostars might evolve along a multiplicity of birthlines with a modest range of luminosity at a given mass.

Our results indicate that there are large uncertainties in assigning ages for the youngest stars from HR diagram positions, given the uncertainty in birthline positions. Our calculations also

suggest that the relatively low disk accretion rates characteristic of T Tauri stars below the birthline cause low-mass stars to contract only slightly faster than normal Hayashi track evolution (Figure 5), so that ages for older pre-main sequence stars estimated from HR diagram positions are relatively secure.

NEAR-INFRARED EMISSION OF PROTOSTARS

In a submitted paper (Calvet, Hartmann, & Strom 1996), we presented models for the thermal emission from dusty infalling envelopes around protostars, which indicate that the envelope emission can greatly exceed the stellar + disk photospheric emission at wavelengths $\sim 2\mu$m. We argued that this thermal envelope emission accounts for the weakness of 2.3μm CO first-overtone absorption lines in protostellar sources (Casali & Eiroa 1996). Disk emission alone is unlikely to explain the observed effect, either because disks exhibit their own CO absorption, or because inner disk holes eliminate the region of the disk which can emit in the near infrared. We find that this near infrared veiling is very dependent on the envelope density, increasing as mass infall rate increases and centrifugal radius decreases. The veiling also depends on the characteristics of the underlying object and it is largest when most of the luminosity is due to accretion and the disk hole size is several stellar radii. The observed veiling indicates that dust must be falling in to distances of ~ 0.1 AU of the central star.

Research plan for third year

1. Infalling Envelopes and Protostars

Our models for protostellar collapse implies that most infalling envelopes of protostars will strongly depart from spherical symmetry. In our initial calculations of thermal equilibrium, we employed spherical averaging to obtain the temperature sturcture of the envelope, but this approximation cannot be correct. Calvet is developing a generalized method of calculating the a 2-D temperature distribution in the case of a dust envelope with axial symmetry, enforcing radiative equilibrium point by point in the envelope. This development is necessary for calculating SEDs in later stages of the collapse of a sheet, in which the density is very angle-dependent and departures of the temperature from the spherically symmetric average are expected to be large. Also, the recent observations of near-infrared veiling among protostellar sources strongly suggest that the in Class I sources is very dependent on the structure of the inner regions of the envelope (Calvet, Hartmann, & Strom 1996), makes it extremely important to have accurate temperature distributions for these regions.

Hartmann and Calvet will pursue hydrodynamic simulations of infall in collaboration with Alan Boss at Carnegie Institution in Washington. Dr. Boss is currently investigating flattened infall models with rotation. We hope to have numerical results in a few months to which we can compare our analytic approximations used in our recent study (Hartmann et al. 1996). We also will explore calculations of scattered light for these numerical models, investigating the possibility that some of the complex structure seen in Hubble Space Telescope images of HL Tau can be explained with these models.

Attention has recently been drawn to so-called "Class 0" objects, which exhibit very red spectra (Andre *et al.* 1993). It has been argued that these objects represent the "youngest"

protostars. However, the Class 0 objects currently known lie in molecular clouds of higher general temperatures, which is predicted to result in larger mass infall rates (Shu 1977; ALS 1987), and higher infall rates naturally result in redder spectral energy distributions (e.g., Kenyon *et al.* 1993a). Hartmann and Calvet will investigate whether the infrared emission of Class 0 objects and other protostellar objects in "warm" molecular cloud regions confirm a basic prediction of protostellar collapse theory - that infall rates increase with the cube of the sound speed in the protostellar cloud (Shu 1977). Hartmann and Calvet will also construct a grid of infall models for higher-mass stars with infalling envelopes, and Hartmann will compare with observations to investigate whether envelopes producing higher-mass stars have larger angular momenta, and thus may produce larger disks.

In the next few months, Calvet will work with a graduate student of the University of Texas and CfA Postdoc Fellow for next year J. DiFrancesco, who will be applying infalling envelope models to the interpretation of his far infrared observations of intermediate mass protostars. This is part of DiFrancesco's PhD thesis, and will be a collaboration with L. Hartmann, Neal Evans and Paul Harvey. the calculations in the next few months.

2. Magnetospheres, Accretion Columns, and Winds of T Tauri Stars

Calvet and a student at UMass, J. Muzerolle, have developed a multilevel atom, 3D radiative transfer code applicable to arbitrary geometries and velocity fields, adopting the Sobolev approximation. This new development is based on the code CV by R. Hewett, which was restricted to a two-level atom approximation. With this code we will calculate fluxes and profiles for optical and infrared lines a grid of models covering a range of mass infall rates, temperatures, and emitting region sizes, with the goals of (1) determining these parameters for stars in T Taurus and comparing the results with determinations from other indicators (i.e., continuum veiling); (2) finding indicators of mass infall rate, temperature, and size, for application to distant/embedded clusters.

Hartmann and Calvet will be working with E. Gullbring (Postdoc at CfA) on calculating the accretion column structure and emission. This development will allow us to assess existing mass infall rate determinations, which usually assume a slab of constant temperature and density. We are planning to propose to HST to obtain UV observations to test our models. It will also enable us, together with our calculations of the magnetospheric flow, to attack the problem of variable excess emission, which seems to originate from accretion rather than surface magnetic activity (Gahm *et al.* 1995), in conjunction with the variability of line profiles.

3. Accretion Disks

Calvet is collaborating with P. D'Alessio (UNAM) on the determination of the structure and emission of steady accretion disks around low-mass young objects, with special emphasis in the calculation of sub/mm and radio fluxes and visibilities. They will study the optically visible T Tauri stars, and with physically-motivated models will determine disk masses and radii (D'Alessio etal, in preparation).

Using the hypothesis of steady accretion, Calvet is working on the interpretation of near infrared fluxes and emission lines of T Tauri stars. M. Meyer (Heidelberg), L. Hillenbrand (Berkeley), and Calvet are using near infrared colors, fluxes, and spectra to determine the range of accretion rates and hole sizes of the disks around these stars.

Our next step is to include the effects of evolution in disks around T Tauri stars. Hartmann, Calvet, and P. D'Alessio are developing time-dependent models which follow the evolution of the disk surface density departing from appropriate boundary conditions. We are initially using similarity solutions for disk evolution to calculate the disk emission properties. These models will be used to compare with recent high spatial resolution HST data and sub/mm and radio observations. Then, we will develop more complicated models, using various viscosity prescriptions in the evolutionary calculations, and compare out model predictions with observations of the decay of mass accretion rate over as large a range of ages as possible, to determine the mechanisms of disk dissipation.

An essential aspect of this study is to develop the most accurate disk accretion rates for T Tauri stars possible, to help constrain disk evolution. We have developed a program of high- and low-resolution spectroscopy and photometry aimed at quantifying disk accretion rates for stars with a wide range of masses and a modest age range. Much of the observing time for this program has already been granted at telescopes on Kitt Peak, Mt. Hopkins, and McDonald Observatory for the coming observing season. We expect data reduction to be finished in the spring and analysis to be completed by summer 1997. L. Hartmann will supervise this work, and these studies will be carried out in collaboration with E. Gullbring, C. Briceño, L. Allen, and S. Strom.

References

Note: * indicates publication supported by this grant

Adams, F.C., Lada, C.J., & Shu, F.H. 1987, ApJ, 312, 788

Andre, P., Ward-Thompson, D., & Barsony, M. 1993, APJ, 406 122

Beckwith, S.V.W., & Birk, C.C. 1995, ApJ, 449, L59

* Calvet, N., Hartmann, L., Kenyon, S., & Whitney, B. 1994, ApJ, 434, 330

* Calvet, N., Hartmann, L., & Strom, S. 1996, ApJ, submitted

Casali, M.M., & Eiroa, C. 1996, A&A, 306, 427

Cassen, P., & Moosman, A. 1981, Icarus, 48, 353

Chick, K.M., Pollack, J.B., & Cassen, P. 1995, ApJ, submitted

* D'Alessio, P., Calvet, N., & Hartmann, L. 1997, ApJ, in press

Gahm, G.F., Loden, K., Gullbring, E., and Hartstein, S. 1995, AA, 301, 89

Gledhill, T.M., & Scarrott, S.M. 1989, MNRAS, 236, 139

Grasdalen, G.L., Sloan, G., Stout, M., Strom, S.E., & Welty, A.D. 1989, ApJL, 339, L37

* Hartmann, L., Boss, A.P., Calvet, N., & Whitney, B. 1994, ApJL, 430, L49

* Hartmann, L., Calvet, N., & Boss, A.P. 1996, ApJ, 464, 387

* Hartmann, L., Cassen, P., & Kenyon, S. 1997, ApJ, in press

Hayashi, M., Ohashi, N., & Miyama, S. 1993, ApJ, 418, L71

* Kenyon, S.J., Calvet, N., & Hartmann, L. 1993a, ApJ, 414, 676

* Kenyon, S.J., & Hartmann, L. 1995, ApJS, 101, 117

* Kenyon, S.J., Whitney, B., Gomez, M., & Hartmann, L. 1993b, ApJ, 414, 773

Lay, O.P., Carlstrom, J.E., Hills, R.E., & Phillips, T.G. 1994, ApJ, 434, L75

Myers, P.C., Fuller, G.A., Goodman, A.A., & Benson, P.J. 1991, ApJ, 376, 561

Nakamura, F., Hanawa, T., & Nakano, T. 1995, ApJ, 444, 770

Palla, F., & Stahler, S.W. 1992, ApJ, 392, 667

Sargent, A.I., & Beckwith, S. 1991, ApJ, 382, L31

Shu, F.H. 1977, ApJ, 214, 488

Stahler, S.W. 1988, ApJ, 332, 804

Stapelfeldt, K.R., Burrows, C.J., Krist, J.E., Trauger, J.T., Hester, J.J., Holtzman, J.A., Ballester, G.E., Casertano, S., Clarke, J.T., Cristp, D., Evans, R.W., Gallagher, J.S. III, Griffiths, R.E., Hoessel, J.G., Mould, J.R., Scowen, P.A., Watson, A.M., & Westphal, J.A. 1995, ApJ, L Aug 20.

Weintraub, D.A., Kastner, J.H., & Whitney, B.A. 1995, preprint

Whitney, B. A., & Hartmann, L. 1993, ApJ, 402, 605

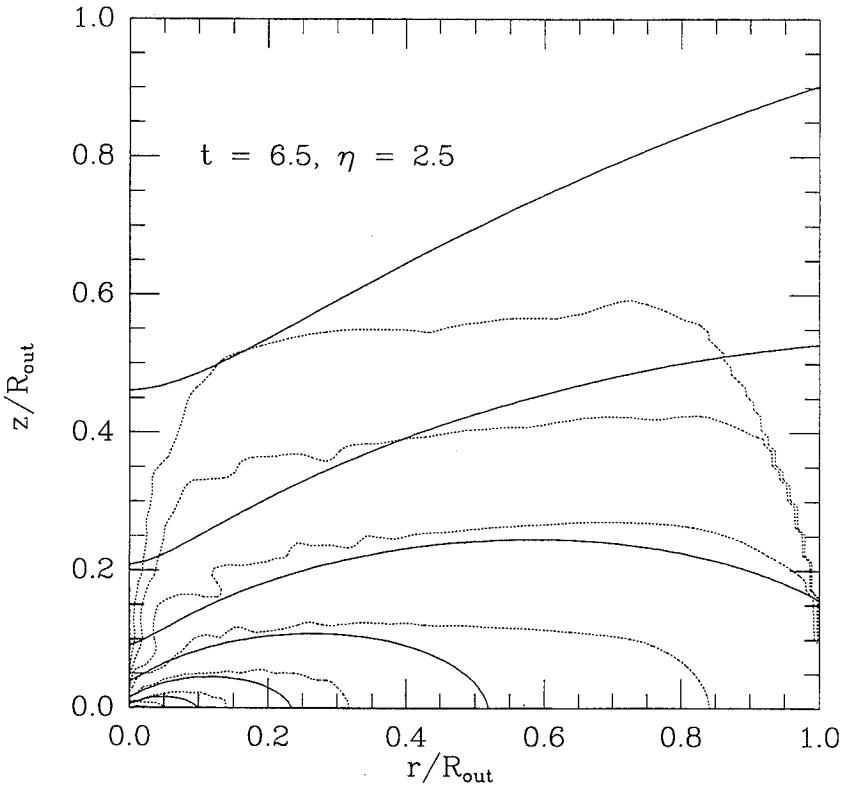

Figure 1: Comparison between the density distributions of the numerical simulation and sheet models. The spatial dimensions are given in units of the outer radius of the cloud $R_{out} = 8.6 \times 10^{16}$ cm. The numerical density distribution at at a time of 6.5 free-fall times $= 3 \times 10^5$ yr is compared with the density distribution of a sheet model characterized by a mass infall rate $6 \times 10^{-6} M_\odot yr^{-1}$, a central mass of $0.21 M_\odot$ (half that of the central mass in the numerical simulation), and $\eta = 2.5$. The lowest density contour corresponds to a molecular hydrogen number density of $10^4 cm^{-3}$, and subsequent contours represent factors of $10^{1/2}$ increase in density.

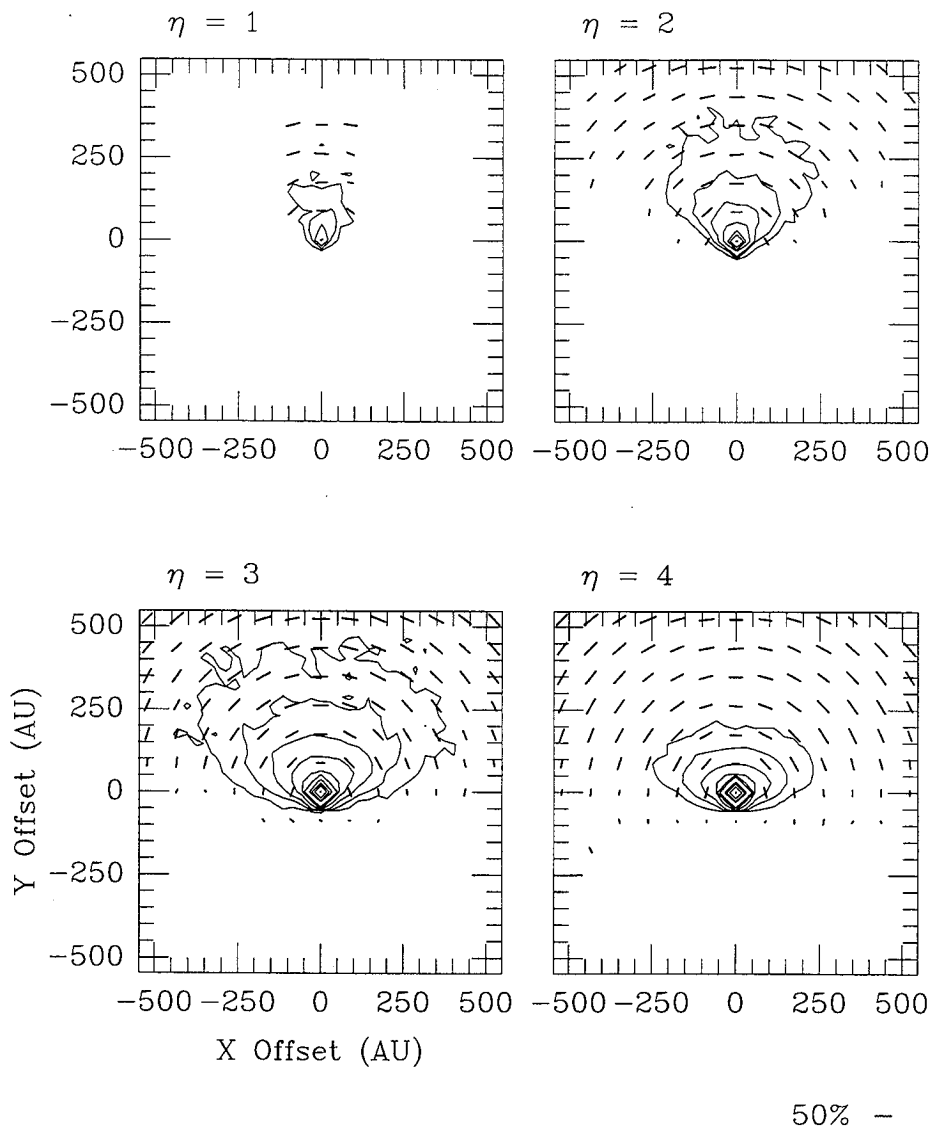

Figure 2: Images and polarization maps at 1.25μm, $i = 60°$, for the $\eta = 1, 2, 3, 4$ models with $\dot{M} = 4 \times 10^{-6} M_{\odot} yr^{-1}$, $R_c = 50$ AU, and $M = 0.5 M_{\odot}$, assuming MRN dust parameters. The opening angle of the reflection nebula increases with increasing η.

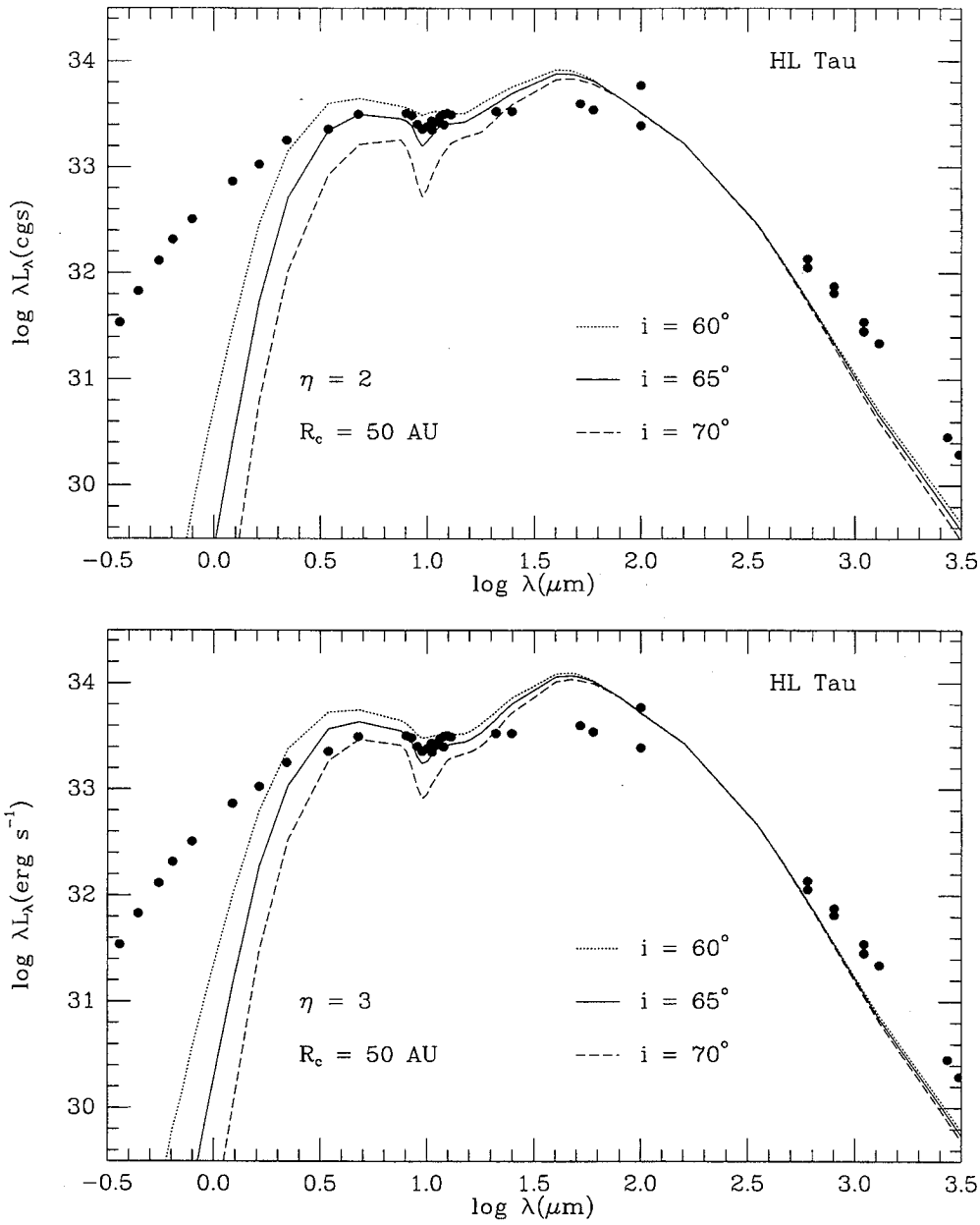

Figure 3: Spectral energy distribution of the flat-spectrum T Tauri star HL Tau (Calvet *et al.* 1994), compared with flattened collapse models with $\eta = 2, 3$ and $R_c = 50$ AU.

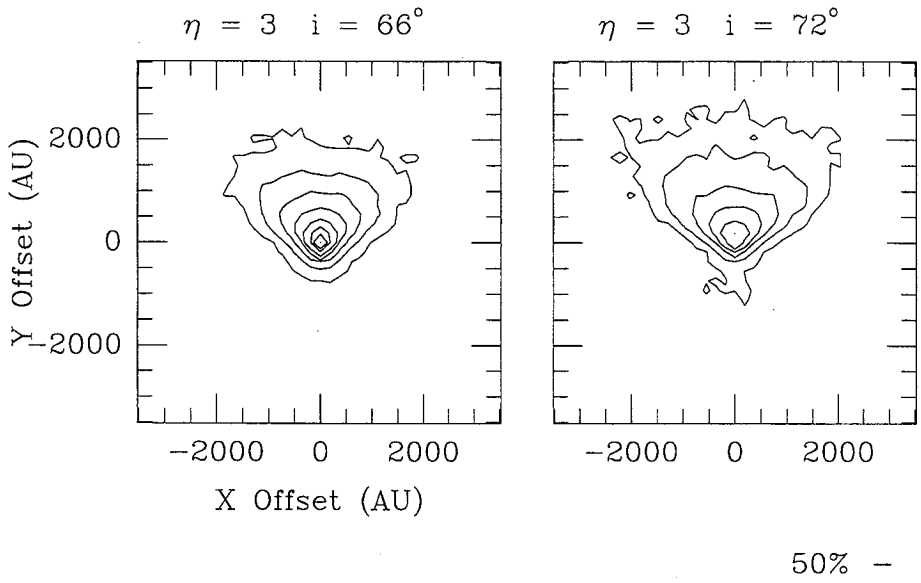

Figure 4: Scattered light calculations at $\lambda = 1.25\mu$ for $\eta = 2, 3$, each at two inclinations, for the HL Tau models (see Figure 3, text).

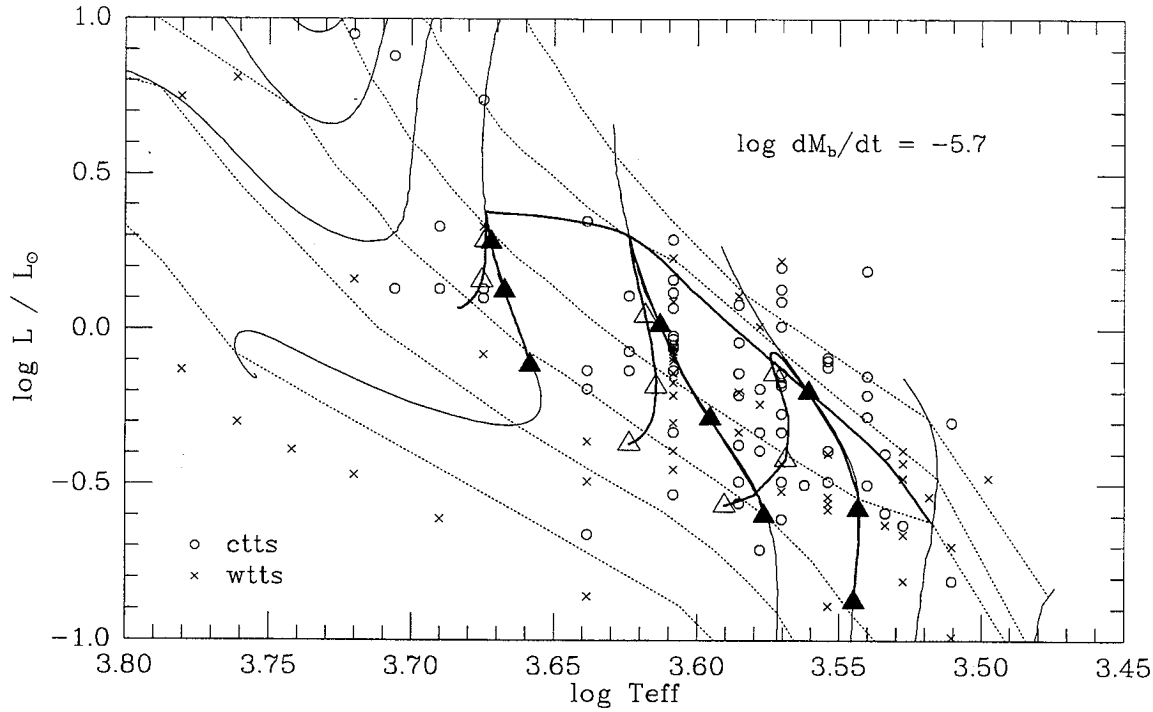

Figure 5: Stellar evolutionary tracks for low-temperature ($\alpha = 0$) disk accretion, compared with observations of T Tauri stars in the Taurus-Auriga star forming region. The evolutionary tracks are calculated interpolating in the CMA results to provide the calibration of $L_{phot}(M, R)$, producing small departures from the power-law calibration results shown in previous figures. The light solid lines show the pre-main sequence evolutionary tracks of D'Antona & Mazzitelli for masses of 0.1, 0.2, 0.3, 0.5, 1, 1.5, 2.0, and 2.5 $M_\odot$. The dashed lines show the D'Antona & Mazzitelli isochrones for 1×10^5 yr, 3×10^5 yr, 1×10^6 yr, 3×10^6 yr, 1×10^7 yr, and 3×10^7 yr. The HR diagram positions of T Tauri stars in the Taurus-Auriga molecular cloud, segregated between weak-emission (WTTS) and strong-emission (CTTS) stars, are taken from Kenyon & Hartmann (1995). (a) The upper heavy solid line corresponds to birthline accretion rate of $\dot{M}_b = 2 \times 10^{-6} M_\odot\,\mathrm{yr}^{-1}$. The lower heavy solid lines show post-birthline evolutionary tracks for zero accretion (connected by solid triangles) and for $\dot{M} = 10^{-7} M_\odot\,\mathrm{yr}^{-1}$ (open triangles). The triangles mark the positions of stars of 0.3, 0.5, and $1.0 M_\odot$ at elapsed times after the end of birthline accretion of 3×10^5, 1×10^6, and 3×10^6 yr. Post-birthline stars may initially move slighly above their birthline positions before descending in the HR diagram (see text).